J. Phys. B: At. Mol. Opt. Phys. **45** (2012) 045001 (6pp) doi:10.1088/0953-4075/45/4/045001

Dielectronic recombination of Au^{20+}: a theoretical description of the resonances at low electron energies

C P Ballance[1], D C Griffin[2], S D Loch[1] and N R Badnell[3]

[1] Department of Physics, Auburn University, Auburn, AL 36849, USA
[2] Department of Physics, Rollins College, Winter Park, FL 32789, USA
[3] Department of Physics, University of Strathclyde, Glasgow, G4 0NG, UK

Received 8 November 2011, in final form 3 January 2012
Published 1 February 2012
Online at stacks.iop.org/JPhysB/45/045001

Abstract
In recent years, there has been significant interest in the dielectronic recombination (DR) of complex ions involving open d and open f subshells. Experimental measurement of DR in Au^{25+} (Hoffknecht *et al* 1998 *J. Phys. B: At. Mol. Opt. Phys.* **31** 2415) and W^{20+} (Schippers *et al* 2011 *Phys. Rev.* A **83** 012711), both with ground configurations of $4p^64d^{10}4f^8$, revealed extremely large and broad resonances at low electron energies. DR in such ions is very difficult to describe in detail theoretically because of the complexity of the recombining resonant states and the source of these resonant structures has not been fully explained for the aforementioned ions. However, a very recent measurement of DR in Au^{20+} (Schippers *et al* 2011 *Phys. Scr.* T **144** 014039) with a ground configuration of $4p^64d^{10}4f^{13}$ displayed very large but narrower resonances in the low-energy region. With the somewhat reduced complexity of the recombining resonances in this ion, we have been able to complete the first full intermediate-coupling level-resolved DR calculation for Au^{20+}. In the low-energy region, we find excellent agreement with the experimental measurements, and have been able to show that the DR rate coefficient in this ion is completely dominated by $\Delta n = 1$ transitions and that the low-energy resonances are primarily due to recombining levels of the $4d^{10}4f^{12}5lnl'$ configurations as suggested by Schippers *et al* (2011 *Phys. Scr.* T **144** 014039) based on atomic structure calculations.

(Some figures may appear in colour only in the online journal)

1. Introduction

There is current interest in the dielectronic recombination (DR) of complex ions involving both open d and open f subshells due to the application of such DR data to plasmas in extreme ultraviolet light sources and controlled nuclear fusion experiments [1], especially ITER. Significant experimental progress has been made on some of these complex ions. Earlier DR measurements were completed by Hoffknecht *et al* [2] on Au^{25+} with a ground configuration of $4p^64d^{10}4f^8$; these were followed recently by measurements of DR for W^{20+} by Schippers *et al* [3], an ion which is isoelectronic to Au^{25+}. Both of these measurements displayed unusually large and broad resonance features at lower electron energies to the extent that no fine individual resonances are distinguishable. Finally, a very recent DR measurement for Au^{20+} by Schippers *et al* [4] with a ground configuration of $4p^64d^{10}4f^{13}$ also revealed large resonances at low electron energies. Here again fine individual resonances were not resolved, but the resonance features were not nearly as broad as those in Au^{25+} or W^{20+}. Based solely on the energies of the resonances determined from atomic structure calculations, Schippers *et al* [4] suggested that these large resonances may be due to the $\Delta n = 1$ transitions to the recombined levels of the $4d^{10}4f^{12}5lnl'$ configurations.

There has been a limited number of theoretical calculations on complex open d subshell ions. For W^{35+} with a ground configuration of $4p^64d^3$, Ballance *et al* [5] presented the results of configuration-average distorted-wave (CADW) calculations of the $\Delta n = 0$ and $\Delta n = 1$ transitions as well as level-resolved distorted-wave and *R*-matrix calculations

for the 4d → 4f and 4p → 4d transitions. The CADW calculations for this ion indicated that the $\Delta n = 1$ contributions to the Maxwellian rate coefficients are not negligible, but are smaller than those arising from the $\Delta n = 0$ transitions at all temperatures. In addition, Badnell *et al* [6] performed DR calculations on the tin ions Sn^{4+} through Sn^{13+} with ground configurations of $4p^64d^q$, with $q = 10$ to 1, using the CADW method, the Burgess–Bethe general program and the level-resolved distorted-wave method. The DR rate coefficients for all of the above ions were found to be dominated by the 4p → 4d and 4d → 4f transitions.

The low-energy DR resonances seen in the measurements for Au^{25+}, W^{20+} and Au^{20+} are very large compared to those found in the theoretical calculations for W^{35+} and Sn^{4+} through Sn^{13+} as discussed above. However, the $4p^64d^{10}4f^8$ configuration present in Au^{25+} and W^{20+} leads to $\Delta n = 0$ and $\Delta n = 1$ resonance structures so complex that level-resolved or even term-resolved calculations on these ions cannot be completed on the largest parallel computer systems presently available. However, the somewhat reduced complexity of the $\Delta n = 0$ and $\Delta n = 1$ resonance structures associated with Au^{20+} makes it possible to perform such calculations.

Although presently, it is not possible to carry out detailed DR distorted-wave calculations for Au^{25+} or W^{20+}, Gribakin *et al* [7], Flambaum *et al* [8] and Gribakin and Sahoo [9] have proposed that the strongly enhanced recombination in these complex ions may not be due to simple DR, but rather recombination from dielectronic states that mix strongly with a very dense spectrum of much more complex multiply excited states. Using statistical theory, they determined an approximate rate for this resonant recombination process in Au^{25+} [8] that agrees with the experimental measurements for this ion [2] above 1 meV. However, in this study we will show that in the less complex case of Au^{20+}, a full level-resolved distorted-wave calculation of DR (without any interactions between the dielectronic states and more complex multiply excited states) does indeed agree with the experimental measurements of Schippers *et al* [3] down to meV electron energies.

2. Calculational methods

In the isolated-resonance approximation, the energy-averaged DR cross section from a state of the initial level i of an N-electron ion through all states of a particular doubly excited level j of the $(N+1)$-electron ion to the states of all possible bound levels f of that ion in atomic units is given by [10]:

$$\bar{\sigma} = \frac{2\pi^2}{\Delta\epsilon k_i^2}\frac{g_j}{2g_i}\frac{\sum_{l_i} A^{\mathrm{a}}(j \to i, k_i l_i)\sum_f A^{\mathrm{r}}(j \to f)}{\sum_{i',l_{i'}} A^{\mathrm{a}}(j \to i', k_{i'} l_{i'}) + \sum_{f'} A^{\mathrm{r}}(j \to f')}. \quad (1)$$

In the above expression, k_i is the linear momentum of the initial continuum electron; $\Delta\epsilon$ is the energy bin width; g_i and g_j are the statistical weights of the initial level of the N-electron ion and the doubly excited level of the $(N+1)$-electron ion, respectively; $A^a(j \to i', k_{i'} l_{i'})$ is the autoionizing rate from a state of the doubly excited level j of the $(N+1)$-electron ion to all lower levels i' of the N-electron ion; and $A^r(j \to f')$ is the radiative rate from a state of the doubly excited level j to all lower levels f' of the $(N+1)$-electron ion. The continuum waves of linear momentum $k_{i'}$ and angular momentum $l_{i'}$ are calculated in the distorted-wave approximation. In equation (1), the sum over f is used to designate bound levels and the sum over f' is used to signify any lower level, including autoionizing levels. By including radiative transitions to autoionizing levels in the denominator, but not the numerator, we provide an approximate correction for the effects of cascades [10].

We have employed a parallel variant of the atomic structure and collisional program AUTOSTRUCTURE developed by Badnell [11–13] to carry out both *LS* term-resolved and Breit–Pauli level-resolved distorted-wave calculations of the DR cross sections and rate coefficients [12] associated with the $4s^24p^64d^{10}4f^{13} \to 4s^24p^64d^{10}4f^{13}$, $4s^24p^64d^{10}4f^{13} \to 4s^24p^64d^94f^{14}$, $4s^24p^64d^{10}4f^{13} \to 4s^24p^64d^94f^{13}5l$ and $4s^24p^64d^{10}4f^{13} \to 4s^24p^64d^{10}4f^{12}5l$ transitions of Au^{20+}. For the *LS* calculation, we also included the $4s^24p^64d^{10}4f^{13} \to 4s^24p^54d^{10}4f^{14}$ and the $4s^24p^64d^{10}4f^{13} \to 4s^24p^54d^{10}4f^{13}5l$ transitions, all of which were found to provide very small contributions to the total DR rate coefficients. We have employed kappa-averaged relativistic orbitals throughout these calculations [14]. Radiative stabilization via either core or Rydberg electron decay was allowed.

These calculations can be parallelized over a user-defined range of angular momentum for the Rydberg electron, though given the scale of work presented here, we have maximized our use of processors by distributing a single Rydberg l to each processor. Although the memory demands are substantial and can be in excess of 40 Gb per Rydberg l, the remaining bottleneck is simply the time required to calculate the high angular momentum Rydberg series and the subsequent post-processing of the Auger and radiative rates. In fact, this calculation required an identical parallelization over Rydberg l of the AUTOSTRUCTURE post-processing code in order to offset the time required to read several terabytes of data. Future work shall investigate a more aggressive degree of parallelization which includes a distribution over principal quantum number as well as the Rydberg l. In this study, for both the term-resolved and level-resolved calculations, we included Rydberg series members up to $n = 75$ to facilitate a closer comparison with the experimental measurement, which reported a field ionization cut-off of $n = 74$.

Theoretical rate coefficients $\langle v\sigma \rangle$ were calculated using both a Maxwellian and an experimental merged-beams velocity distribution in the centre-of-mass frame of the ion, given by [12]

$$f(v_0, \mathbf{v}) = \left\{\frac{m_e}{2\pi kT_\parallel}\right\}^{\frac{1}{2}} \exp\left(-\frac{m_e(v_\parallel - v_0)^2}{2kT_\parallel}\right)\frac{m_e}{2\pi kT_\perp} \times \exp\left(-\frac{m_e(v_\perp)^2}{2kT_\perp}\right), \quad (2)$$

where $v_0 = \sqrt{(2E_0/m_e)}$ and E_0 is the electron–ion centre-of-mass energy; $T_\perp$ and $T_\parallel$ are the temperatures corresponding to motion perpendicular and parallel to the ion beam, respectively; finally, $v_\perp$ and $v_\parallel$ correspond to the perpendicular and parallel components of $\mathbf{v}$.

Although the capability to carry out level-resolved DR calculations for open d and f subshell systems using perturbative methods is beginning to emerge, they remain time and resource intensive. Therefore, it is beneficial to have a simpler method such as the CADW approach to guide the more sophisticated approaches and to indicate where to focus subsequent efforts. With the CADW method, we simply replace the level-resolved autoionizing and radiative rates in equation (1) with rates calculated in the configuration-average approximation:

$$\bar{\sigma}_{\mathrm{CA}} = \frac{2\pi^2}{\Delta\epsilon k_i^2}\frac{G_j}{2G_i}\frac{\sum_{l_i}\bar{A}^{\mathrm{a}}(j\rightarrow i,k_il_i)\sum_f \bar{A}^{\mathrm{r}}(j\rightarrow f)}{\sum_{i',l_{i'}}\bar{A}^{\mathrm{a}}(j\rightarrow i',k_{i'}l_{i'})+\sum_{f'}\bar{A}^{\mathrm{r}}(j\rightarrow f')}, \tag{3}$$

where G_i and G_j are the total statistical weights of the N-electron configuration of the initial ion and the doubly excited configuration of the $(N+1)$-electron ion, respectively; $\bar{A}^a(j \rightarrow i', k_{i'}l_{i'})$ is the configuration-average autoionizing rate from a state of the doubly excited $(N+1)$-electron configuration j to all states of configuration i' of the N-electron ion; and $\bar{A}^r(j \rightarrow f')$ is the configuration-average radiative rate from a state of the doubly excited configuration j to all states of the lower configuration f' of the $(N+1)$-electron ion. Details regarding the equations for calculating the configuration-average rates are provided in Griffin *et al* [10] and the derivation of these equations is presented in Pindzola *et al* [15]. An extensively modified version of the program DRACULA, which was first developed many years ago [10] was employed here for all CADW calculations; this modified version of DRACULA is described in Ballance *et al* [5].

We first carried out a series of CADW Maxwellian rate coefficient calculations that included the DR transitions associated with the 4p $\rightarrow$ 4f, 4d $\rightarrow$ 4f, 4p $\rightarrow$ 5*l*, 4d $\rightarrow$ 5*l* and 4f $\rightarrow$ 5*l* transitions. In these calculations, the maximum values of n and l for the Rydberg electron were set to 1000 and 12, respectively. It was found that the contributions due to excitations from the 4p subshell were completely negligible and that the rate coefficients were completely dominated by the $\Delta n = 1$, 4d $\rightarrow$ 5*l* and 4f $\rightarrow$ 5*l* transitions.

We then performed a term-resolved AUTOSTRUCTURE DR calculation of the rate coefficient as measured in the merged-beam experiment by Schippers *et al* [4] that included the same transitions listed above for the CADW calculation. The values of $kT_{||}$ and $kT_{\perp}$ (in equation (2)) were set equal to 0.1 and 10.0 meV, respectively, corresponding to the values given in the experiment. As indicated above, the maximum value of n for the Rydberg electron was set equal to 75, while the maximum value of l was set to 7. Again, it was found that the contributions due to excitations from the 4p subshell were completely negligible.

Finally, we performed a much larger level-resolved AUTOSTRUCTURE DR calculation of the rate coefficient as measured in the merged-beam experiment. On the basis of the results of the CADW and term-resolved calculations, we eliminated all excitations from the 4p subshell, which was required to make this calculation feasible. Again the values of $kT_{||}$ and $kT_{\perp}$ were set equal to 0.1 and 10.0 meV, respectively, and the maximum values of n and l for the Rydberg electron were set to 75 and 7, respectively.

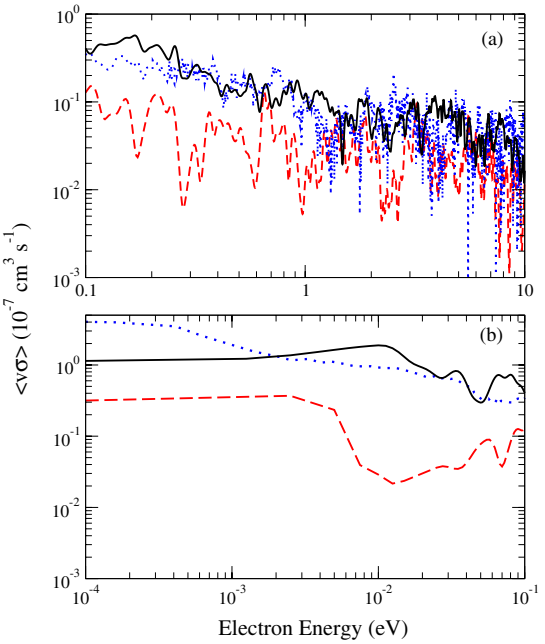

Figure 1. Dielectronic recombination rate coefficient for Au^{20+} as measured in the merged-beam experiment in (a) the higher energy range and (b) the low-energy range. The y-axis is labelled $\langle v\sigma \rangle$ to distinguish it from a Maxwellian rate coefficient. The electron-beam temperatures are $kT_{||} = 0.1$ meV and $kT_{\perp} = 10.0$ meV. The dotted (blue) curves are from the experimental measurements of Schippers *et al* [4]; the dashed (red) curves are from the present term-resolved, *LS*-coupling calculation and the solid (black) curves are from the present level-resolved, intermediate-coupling calculation.

3. Results

In figure 1, the results for both the term-resolved and level-resolved distorted-wave calculations are compared to the experimental measurements for energies from 0.1 up to 10.0 eV (which is the maximum energy reported in the experimental paper) in (a) and from 10^{-4} to 0.1 eV in (b). As can be seen, the resonance structure associated with the term-resolved calculation is quite pronounced in (a) and it persists to quite low energies in (b); however, it is significantly lower than that determined from the experiment in both energy ranges. On the other hand, the level-resolved calculation leads to resonances of the same magnitude as those determined from the merged-beam measurements in (a) and this agreement between theory and experiment continues down to an energy of about 2×10^{-3} eV in (b).

Below approximately 2×10^{-3} eV, the experiment is clearly above theory, and at an energy of 10^{-4} eV, the experimental rate coefficient is about four times that from the intermediate-coupling calculation. However, this discrepancy is most likely due to an additional enhancement of recombination below approximately an meV that has been observed in many of these merged-beam experiments. This enhancement is found even in bare ions where DR is not possible [16] and is found to be a function of $kT_{||}$, $kT_{\perp}$ and the magnetic field [17]. This explanation of the very low energy discrepancy in Au^{20+} is further supported by the fact that, in

the case of Au^{25+}, the experimental rate coefficient below a few milli-electron volts is observed to vary significantly with magnetic field strength [2].

Thus, a full level-resolved distorted-wave calculation is capable of explaining the experimental measurements for this complex species to very low energies. It is also important to note that the theoretical rate coefficient throughout these two energy regions is completely dominated by resonances associated with the $4d^{10}4f^{12}5lnl'$ configurations, as suggested by Schippers *et al* [4].

Since the level-resolved calculation appears to be an accurate description of the experiment, it would also be desirable to calculate Maxwellian rate coefficients over a wide temperature range in full intermediate coupling. However, we first had to determine whether the limits on the maximum values of n and l for the Rydberg electron of 75 and 7, respectively, used in the level-resolved calculation are sufficient. To go beyond these limits would make an already large and time consuming calculation untenable. Thus, we repeated the CADW calculation over these lower limits and compared the resulting rate coefficients with those determined from our earlier CADW rate coefficients with an n limit of 1000 and an l limit of 12. We compare these rates in figure 2, where we have included only the $\Delta n = 0$ excitations out of the 4d subshell and the $\Delta n = 1$ excitations out of the 4d and 4f subshells, since excitations out of the 4p subshell make a negligible contribution to the rate coefficient. As can be seen, the differences between these sets of rate coefficients are relatively small. For example, at 10 eV the differences in the total rate coefficients are completely negligible, at 100 eV they differ by 5% and at 1000 eV they differ by 17%.

Based on these results, we generated level-resolved Maxwellian rate coefficients and compared them with those determined from the CADW method. This comparison is shown in figure 3, where the individual level-resolved rate coefficients in (a) were determined using the capability of the AUTOSTRUCTURE post-processing code to isolate the contribution to the total DR rate from the Rydberg sequences attached to the levels associated with a particular excited core, and where the CADW rate coefficients in (b) are from the calculation with the lower n and l limits.

An approximate ionization balance calculation for Au was also performed using the Atomic Data and Analysis Structure (ADAS) codes [18]. Since no accurate ionization or recombination rate coefficients exist for many of the ion stages of gold, particularly those close to Au^{20+}, this calculation employed the Lotz formula for ionization and the Burgess general formula for recombination. The accuracy of this calculation was also adversely affected by uncertainties in the ground states, and thereby the ionization potentials of some of the neighbouring Au ions. However, it predicted that Au^{20+} is most prevalent between about 130 and 300 eV; this range of temperatures is shown in figure 3 by the horizontal solid lines.

Although the total rate coefficients from the level-resolved and CADW calculations are reasonably close, this is largely fortuitous since the individual rates corresponding to the 4d $\rightarrow$ 4f, the 4d $\rightarrow$ 5l and the 4f $\rightarrow$ 5l excitations differ significantly. In the case of the level-resolved calculation,

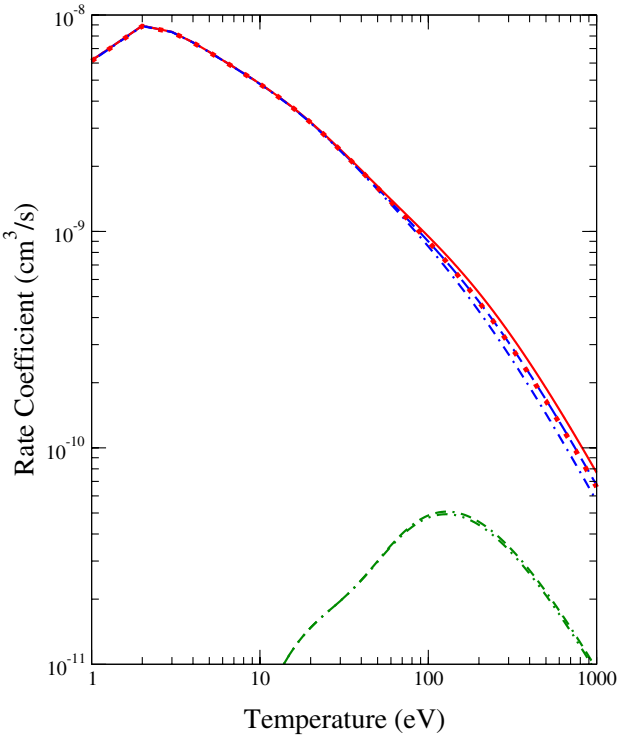

Figure 2. Comparisons of configuration-average dielectronic recombination Maxwellian rate coefficients for which the maximum n and l values of the Rydberg electrons were set at 1000 and 12, respectively, with the rate coefficients for which the maximum n and l values were set at 75 and 7, respectively. The double-dashed-dot (green) curve is the $\Delta n = 0$ rate with the higher values of n and l; the dashed-double-dot (green) curve is the $\Delta n = 0$ rate with the lower values of n and l; the dashed (blue) curve is the $\Delta n = 1$ rate with the higher values of n and l; the dashed-dot (blue) curve is the $\Delta n = 1$ rate with the lower values of n and l; the solid (red) curve is the total rate with the higher values of n and l and the dotted (red) curve is the total rate with the lower values of n and l.

the rate coefficient associated with the 4f $\rightarrow$ 5l excitation completely dominates up to a temperature of about 50 eV, and even at 1000 eV it provides about 65% of the total rate coefficient. It is also worth noting that the levels associated with the $4d^{10}4f^{12}5pnl'$ configuration provide the largest contribution associated with the 4f $\rightarrow$ 5l excitations, followed by the contributions from levels of the $4d^{10}4f^{12}5dnl'$ and $4d^{10}4f^{12}5fnl'$ configurations. The total Maxwellian-averaged level-resolved DR rate coefficient has been fitted and the associated coefficients are defined and given in table 1.

In the case of the CADW rate coefficients, both the 4d $\rightarrow$ 5l and the 4f $\rightarrow$ 5l excitations contribute significantly. This is partially due to the fact that in the CADW calculation there is an extremely large resonance arising from the $4p^64d^94f^{13}5s5f$ configuration, which lies at an energy of only 3.0 eV, and yet dominates the 4d $\rightarrow$ 5l rate coefficient to quite high temperatures. If this particular resonance is eliminated from the calculation, then the CADW 4d $\rightarrow$ 5l rate coefficient is very small at lower temperatures and is significantly reduced at higher temperatures.

This points out the most significant difficulty with the CADW method; in the configuration-average approximation,

Table 1. Fitting coefficients to the total Maxwellian averaged Au^{20+} DR rate coefficient as presented in figure 3(a); $\alpha(T_e) = T_e^{-3/2} \sum_i c_i \exp(-E_i/kT_e)$. The fit is valid to within 2% within the energy range 1 to 1000 eV. The c_i are given in units of $K^{3/2}$ cm^3 s^{-1} and E_i is given in eV.

c_i	4.160(−2)	1.489(−1)	4.121(−1)	6.178(−1)	1.066(+0)	1.073(+0)	5.878(−1)
E_i	8.743(−1)	6.629(+0)	3.314(+1)	1.173(+2)	2.710(+2)	2.710(+2)	4.272(+2)

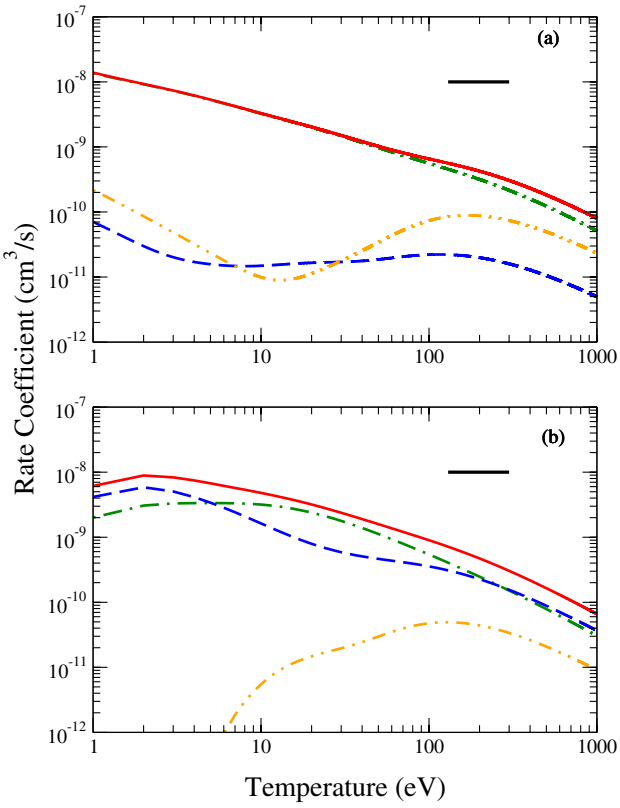

Figure 3. Dielectronic recombination Maxwellian rate coefficients from the present intermediate-coupling calculations in (a) and the present configuration-average calculations in (b). For both (a) and (b), the dashed-double-dot (orange) curves are the rates associated with the 4d → 4f transition; the dashed (blue) curves are the rates associated with the 4d → 5*l* transitions; the dashed-dot (green) curves are the rates associated with the 4f → 5*l* transitions; and the solid (red) curves are the total rates. The solid horizontal (black) lines in both (a) and (b) show the approximate range of temperatures where the Au^{20+} ion should be most abundant under equilibrium conditions.

a particular resonance may occur just above or just below the energy of the ground configuration of the initial *N*-electron ion; if just below, it makes no contribution to the DR rate, while if just above, it can make a significant contribution. On the other hand, a term-resolved or level-resolved calculation will spread the resonances arising from this configuration over a wide energy range, some with energies below the ground level of the initial *N*-electron ion and some above. Thus, the primary advantage of the CADW method is that it provides a quick way of estimating various DR contributions before more sophisticated methods are attempted. When term-resolved or level-resolved calculations are not possible, it still can provide approximate values of rate coefficients at higher temperatures.

4. Conclusions

We have completed level-resolved intermediate-coupling distorted-wave calculations of dielectronic recombination for Au^{20+} that agree very well with the results of a merged-beam experiment for this ion. We have also confirmed the identification of the large low-energy resonances proposed by Schippers *et al* [4]. Clearly, the inclusion of interactions between the dielectronic states and a high density of more complex multi-electron states as proposed to explain recombination in Au^{25+} [7–9] is not required in Au^{20+}.

Since atomic data for the ions of tungsten are of significant interest for the modelling of impurity transport and radiative power loss in ITER, DR calculations for many tungsten ions are urgently needed. Full level-resolved or even term-resolved calculations for ions such as W^{20+} are presently not possible even with the parallel computer systems currently available. However, level-resolved calculations for W^{27+} with a ground configuration of $4p^64d^{10}4f$ are entirely possible. In addition, term-resolved calculations and perhaps even level-resolved calculations are possible for W^{26+} with a ground configuration of $4p^64d^{10}4f^2$. Thus, merged-beam measurements on either or both of these ions would be very beneficial.

Acknowledgments

This work was supported in part by DOE grants to Auburn University and a Euratom Framework 7 Support Action Agreement with the University of Strathclyde. Some of the computational work was performed at the National Energy Research Scientific Computer Center in Oakland CA and the Alabama Supercomputer Center. We would like to thank Dr Stefan Schippers for providing the tabulated experimental data presented in figure 1.

References

[1] Pütterich T, Neu R, Dux R, Whiteford A D and O'Mullane M G 2008 and the ASDEX Upgrade Team *Plasma Phys. Control. Fusion* **50** 085016
[2] Hoffknecht A *et al* 1998 *J. Phys. B: At. Mol. Opt. Phys.* **31** 2415
[3] Schippers S *et al* 2011 *Phys. Rev.* A **83** 012711
[4] Schippers S *et al* 2011 *Phys. Scr.* T **144** 014039
[5] Ballance C P, Loch S D, Pindzola M S and Griffin D C 2010 *J. Phys. B: At. Mol. Opt. Phys.* **43** 205201
[6] Badnell N R, Foster A, Griffin D C, Kilbane D, O'Mullane M and Summers H P 2011 *J. Phys. B: At. Mol. Opt. Phys.* **44** 135201
[7] Gribakin G F, Gribakina A A and Flambaum V V 1999 *Aust. J. Phys.* **52** 443
[8] Flambaum V V, Gribakina A A, Gribakin G F and Harbati C 2002 *Phys. Rev.* A **66** 012713

[9] Gribakin G F and Sahoo S 2003 *J. Phys. B: At. Mol. Opt. Phys.* **36** 3349
[10] Griffin D C, Pindzola M S and Bottcher C 1985 *Phys. Rev.* A **31** 568
[11] Badnell N R 1986 *J. Phys. B: At. Mol. Opt. Phys.* **19** 3827
[12] Badnell N R 2006 *J. Phys. B: At. Mol. Opt. Phys.* **39** 4825
[13] Badnell N R 2011 *Comput. Phys. Commun.* **182** 1528
[14] Cowan R D and Griffin D C 1976 *J. Opt. Soc. Am.* **66** 1010
[15] Pindzola M S, Griffin D C and Bottcher C 1986 Atomic processes in electron–ion and ion–ion collisions *NATO ASI* B **145** 75
[16] Gao H, Schuch R, Zong W, Justiniano E, DeWitt D R, Lebius H and Spies W 1997 *J. Phys. B: At. Mol. Opt. Phys.* **30** L499
[17] Gwinner G *et al* 2000 *Phys. Rev. Lett.* **84** 4822
[18] http://www.adas.ac.uk